On the Utility of the Circular Ring Model for Wideband MIMO Channels

Zoran Latinovic, Ali Abdi and Yeheskel Bar-Ness
Center for Communication and Signal Processing Research, Dept. of Elec. and Comp. Eng.
New Jersey Institute of Technology, University Heights, Newark, NJ 07102
Email: {zl3, ali.abdi, barness}@njit.edu.

***Abstract*— In this paper, we use the circular ring scattering model to derive the signal statistics of a wideband MIMO channel. Based on the proposed model, a new space–time–frequency cross–correlation (STF) function is derived for the MIMO channel. The cross–correlation includes various parameters of interest such as the distance between the base station and the user, spacing among antenna elements, user's speed and direction, as well as the angle spread and delay spread. In addition, the important channel properties such as the time of arrival PDF and power delay profile as well as the angle of arrival probability density function (PDF) and power azimuth spectrum are derived and compared with measured data. The proposed model and associated wideband STF cross–correlation provide a convenient unified framework for the characterization and simulation of frequency selective mobile MIMO fading channels and the design of proper STF codes and signaling techniques over such channels.**

I. Introduction

Multiple-input multiple-output (MIMO) wireless systems have multiple antennas at both receiver and transmitter. Under the condition of uncorrelated antenna elements and Rayleigh fading, capacity of the system can be increased linearly with the number of antennas. Most of the theoretical works in the past [1]–[3] assumed that kind of simplified channel model, but in practice some correlation among the antenna elements may exist that can reduce the channel capacity.

Moreover, most papers in the past have focused on frequency-flat fading channels, whereas frequency selective channels have recently received significant attention due to the high demand for high data rate communications [4], [5].

In [6] we demonstrated that the circular ring model exhibits good match to temporal characteristics of wideband measured channel data such as time of arrival (TOA) probability density function(PDF) and power delay spectrum (PDS), also known as power delay profile.

The main contribution of this paper is the derivation of all the channel characteristics of interest not discussed in [6], namely angle of arrival (AOA) PDFs and power azimuth spectrum (PAS) at both the base station (BS) and user side. The effect of path-loss in included as well as its impact on PASs and the PDS. A corresponding closed-form space-time-frequency (STF) cross-correlation function among the links of a frequency selective MIMO mobile fading channel is also derived.

This work was supported in part by NSF under Grant CCR-0085846.

The rest of this paper is organized as follows. The circular ring wideband geometric-stochastic model for MIMO channels is briefly introduced in Section II, whereas the new STF cross-correlation is derived in Section III. Section IV is devoted to the derivation of relevant channel properties of the circular ring model. Their comparison with published wideband measurements is the topic of Section V. Concluding remarks are given in Section VI.

II. The Circular Ring Wideband MIMO Model

Consider the multi-element antenna system configuration, shown in Fig. 1, where the BS and the user have n_{BS} and n_U omni-directional antenna elements in the horizontal plane, respectively. Without loss of generality, the case of $n_{BS} = n_U = 2$ (a 2×2 MIMO channel) has been considered. The BS receives the signal through the narrow beamwidth $2\Delta_2$, while the user receives the signal from a large number of surrounding local scatterers, impinging the user from different directions. We assume that the waves are bounced only once. The i^{th} scatterer is represented by S_i, R_i is the distance between the S_i and user, and D is the distance between the BS and user. All scatterers are located within the circular ring, with the distance from the user within the range $R_1 \le R_i \le R_2$. Clearly, Δ_2, R_2, and D are related through $\sin(\Delta_2) = R_2/D$.

In the channel model depicted in Fig. 1, the local scatterers are assumed to be fixed, independent of time, and the motion of the user is characterized by its speed $\mathbf{v}$, i.e., the intensity $\mathrm{v} = |\mathbf{v}|$ and direction $\gamma = \measuredangle\mathbf{v}$. These assumptions are necessary for obtaining a stationary STF correlation function. The same assumptions can be found, for example, in [7] and [8] for the temporal correlation model, and in [9] and [10] for the spatio-temporal correlation model. Clearly, depending on the users speed, the STF correlation function derived in the next section will be accurate only over a time duration that is much smaller than R_1/v.

Let us define the power transferred through the $BS_p - U_l$ link as Ω_{lp}, where $\Omega_{lp} = E\big[\,|h_{lp}(\tau,t)|^2\,\big] \le 1$, under the assumption of the unit total transmit power. The waves emitted from the array element BS_p travel over paths with different lengths and after being scattered by the local scatterers around the mobile user, impinge the array element U_l from different

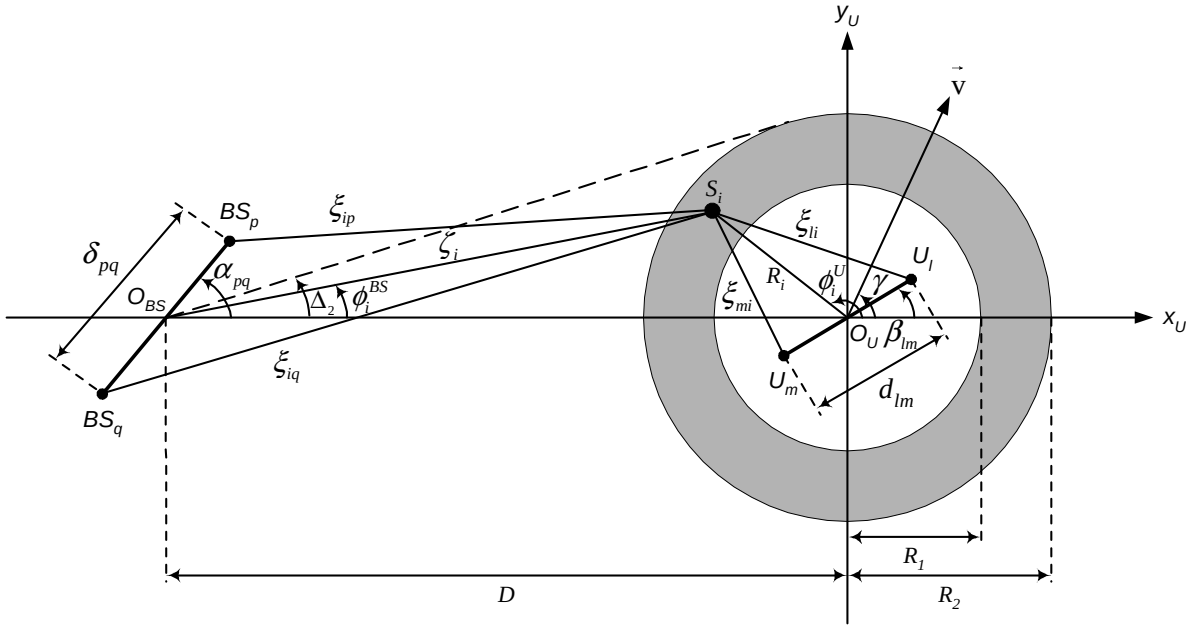

Fig. 1. Geometrical configuration of a 2 × 2 circular ring channel with local scatterers around the mobile user (two-element arrays at the BS and user side).

directions. Since we consider the Rayleigh fading channel, no line-of-sight (LOS) component exists. Mathematical representation of this propagation mechanism, results in the following expression

$$h_{lp}(\tau,t) = \lim_{N\to\infty} \frac{1}{\sqrt{N}} \sum_{i=1}^{N} g_i \left(2\pi\zeta_i \cdot 2\pi R_i\right)^{-n/2} \exp\left\{j\psi_i - j2\pi\lambda^{-1}\left(\xi_{ip}+\xi_{li}\right) + j2\pi f_D t\cos\left(\phi_i^U-\gamma\right)\right\}\delta(\tau-\tau_i). \tag{1}$$

In the formula above, N is the number of independent scatterers S_i around the user, g_i represents the amplitude of the wave scattered by the S_i toward the user. The phase shift introduced by the S_i is denoted by ψ_i, ξ_{ip} and ξ_{li} are the distances shown in the Fig. 1, which are functions of ϕ_i^U and R_i. For $d_{lm} \ll R_1$, the term $(2\pi\xi_{ip}\cdot 2\pi\xi_{li})$ related to the amplitude attenuation can be replaced with $(2\pi\zeta_i \cdot 2\pi R_i)$. However, replacing $\xi_{ip}\,(\xi_{li})$ with $\zeta_i\,(R_i)$ in the exponent is inappropriate due to non-negligible phase shifts. Further, the wavelength is denoted by λ, $j^2=-1$, c stands for the speed of light, $f_D = \mathrm{v}/\lambda$ is the maximum Doppler shift, n represents the path-loss exponent and finally τ_i is the travel time of the wave scattered by the S_i.

III. The New Space-Time-Frequency Cross-Correlation

The time-varying frequency response $T(f,t)$ is defined in [11] as the Fourier transform (FT) of $h(\tau,t)$, i.e., $T(f,t) = \mathcal{F}_\tau\{h(\tau,t)\}$. For the communication link $BS_p - U_l$ we have

$$T_{lp}(f,t) = \lim_{N\to\infty} \frac{(2\pi)^{-n}}{\sqrt{N}} \sum_{i=1}^{N} g_i \left(\zeta_i \cdot R_i\right)^{-n/2} \exp\left\{j\psi_i - j2\pi\lambda^{-1}\left(\xi_{ip}+\xi_{li}\right) + j2\pi f_D t\cos\left(\phi_i^U-\gamma\right) - j2\pi f\tau_i\right\}. \tag{2}$$

Now we define the normalized STF cross-correlation function between the time-varying frequency responses of two arbitrary communication links $T_{lp}(f,t)$ and $T_{mq}(f,t)$ as

$$\rho_{lp,mq}\left(\Delta f,\Delta t\right) = \frac{E[T^*_{mq}(f,t)T_{lp}(f+\Delta f,t+\Delta t)]}{\sqrt{\Omega_{mq}\Omega_{lp}}} \tag{3}$$

where $(\cdot)^*$ denotes the complex conjugate operation. The definition is slightly different from [6, eq. 4] in order to make it in accordance with [11], [12]. Following a similar approach to the one given in [6], i.e., assuming independence between the ϕ^U and R, $\Omega_{mq} = \Omega_{lp} = \Omega$, von Mises PDF for the AOA at the user side (4),

$$f\left(\phi^U\right) = \frac{\exp\left[\kappa\cos\left(\phi^U-\mu\right)\right]}{2\pi I_0(\kappa)}, \quad \phi^U \in [-\pi,\pi) \tag{4}$$

and a number of approximate relations such as $\sqrt{1+x} \approx 1+x/2$, $\sin(x)\approx x$, $\cos(x)\approx 1$, $(1+x)^{-n}\approx 1-nx$ valid for small x and $n>0$, the STF cross-correlation can be expressed by (5),

$$\begin{aligned}\rho_{lp,mq}(\Delta f,\Delta t) \approx{}& \frac{(2\pi)^{-2n}D^{-n}}{\Omega I_0(\kappa)} \\ &\times \int_{R_1}^{R_2} \exp\left[jc_{pq}\cos(\alpha_{pq}) - jz\left(1+\Delta^{-1}\right)\right] \\ &\times \left\{I_0\left(\sqrt{x^2+y^2}\right) - n\Delta\frac{x}{\sqrt{x^2+y^2}} I_1\left(\sqrt{x^2+y^2}\right)\right\} \\ &\times R^{-n} f(R) dR.\end{aligned} \tag{5}$$

To simplify notation, x and y are defined as,

$$\begin{aligned} x &= \kappa\cos(\mu) + j\left[b_{lm}\cos(\beta_{lm}) + a\cos(\gamma) - z\right], \\ y &= \kappa\sin(\mu) + j\left[c_{pq}\Delta\sin(\alpha_{pq}) + b_{lm}\sin(\beta_{lm}) + a\sin(\gamma)\right], \end{aligned}$$

$$f\left(\phi^{BS}\right) \approx \begin{cases} \frac{1}{\pi I_0(\kappa)} \int\limits_{\Delta_1}^{\Delta_2} \exp\left(\frac{\kappa}{\Delta}\sin(\mu)\phi^{BS}\right) \frac{\cosh\left(\frac{\kappa}{\Delta}\cos(\mu)\sqrt{\Delta^2-(\phi^{BS})^2}\right)}{\sqrt{\Delta^2-(\phi^{BS})^2}} f(\Delta)d\Delta, & \left|\phi^{BS}\right| \le \Delta_1 \\ \frac{1}{\pi I_0(\kappa)} \int\limits_{|\phi^{BS}|}^{\Delta_2} \exp\left(\frac{\kappa}{\Delta}\sin(\mu)\phi^{BS}\right) \frac{\cosh\left(\frac{\kappa}{\Delta}\cos(\mu)\sqrt{\Delta^2-(\phi^{BS})^2}\right)}{\sqrt{\Delta^2-(\phi^{BS})^2}} f(\Delta)d\Delta, & \Delta_1 < \left|\phi^{BS}\right| \le \Delta_2 \end{cases} \tag{6}$$

$$P\left(\phi^{BS}\right) \approx \begin{cases} \frac{(2\pi D)^{-2n}}{\Omega\pi I_0(\kappa)} \cos\left(\phi^{BS}\right) \int\limits_{\Delta_1}^{\Delta_2} \exp\left(\frac{\kappa}{\Delta}\sin(\mu)\sin\left(\phi^{BS}\right)\right) \left[\frac{\cosh\left(\frac{\kappa}{\Delta}\cos(\mu)\sqrt{\Delta^2-\sin(\phi^{BS})^2}\right)}{\sqrt{\Delta^2-\sin(\phi^{BS})^2}}\right. \\ \qquad \left. -n\sinh\left(\frac{\kappa}{\Delta}\cos(\mu)\sqrt{\Delta^2-\sin\left(\phi^{BS}\right)^2}\right)\right] \Delta^{-n} f(\Delta)d\Delta, \qquad \left|\sin\left(\phi^{BS}\right)\right| \le \Delta_1 \\ \frac{(2\pi D)^{-2n}}{\Omega\pi I_0(\kappa)} \cos\left(\phi^{BS}\right) \int\limits_{|\sin(\phi^{BS})|}^{\Delta_2} \exp\left(\frac{\kappa}{\Delta}\sin(\mu)\sin\left(\phi^{BS}\right)\right) \left[\frac{\cosh\left(\frac{\kappa}{\Delta}\cos(\mu)\sqrt{\Delta^2-\sin(\phi^{BS})^2}\right)}{\sqrt{\Delta^2-\sin(\phi^{BS})^2}}\right. \\ \qquad \left. -n\sinh\left(\frac{\kappa}{\Delta}\cos(\mu)\sqrt{\Delta^2-\sin\left(\phi^{BS}\right)^2}\right)\right] \Delta^{-n} f(\Delta)d\Delta, \qquad \Delta_1 < \left|\sin\left(\phi^{BS}\right)\right| \le \Delta_2 \end{cases} \tag{8}$$

where $a = 2\pi f_D \Delta t$, $b_{lm} = 2\pi d_{lm}/\lambda$, $c_{pq} = 2\pi\delta_{pq}/\lambda$, $z = 2\pi R\Delta f/c$ and $\Delta = R/D$. For a given $f(R)$, the cross-correlation function in (5) needs to be calculated, numerically.

IV. Model Properties

In order to derive the mentioned model properties and compare them to the available measured data [13], we need to consider the single-input single-output (SISO) version of the model by setting $d_{lm} = \delta_{pq} = 0$. While the TOA and PDS are the same for the BS and user side, the AOA and PAS differ significantly with respect to the side of observation. In the following subsections, expressions for all the relevant model properties are derived.

A. PDF of Angle of Arrival

We assumed earlier that the AOA at the user side resembles von Mises PDF (4).

For small ϕ^{BS}, the AOA seen from the BS side can be approximated by $\phi^{BS} \approx \Delta\sin\left(\phi^{U}\right)$. Calculating the conditional PDF $f\left(\phi^{BS}\middle|\,\Delta\right)$ from ϕ^{BS} and (4), multiplying it by $f(\Delta)$ and doing integration over all values of Δ gives the final expression of the AOA PDF at the BS given by (6), where $\Delta_1 = R_1/D$ and $\Delta_2 = R_2/D$.

B. Power Azimuth Spectrum

The PAS can be found from the STF cross-correlation (5) using the FTs given in [12, eq. (45)]. Expression (45) gives the relation between the PAS $P(\phi)$ and $\tilde{\phi}$ direction-constained space correlation $R_{\tilde{\phi}}(\Delta d)$.

In the case of PAS seen by the user side being of interest, the spatial correlation $R^U_{\tilde{\phi}}(\Delta d)$ equals to (5) simply by setting $a = c_{pq} = z = 0$, $\Delta d = d_{lm}$ and $\tilde{\phi} = \beta_{lm}$. According to the basic properties of the Bessel functions, FT pair given in [14, 3.3-12, p. 124] and simple trigonometric identities gives the PAS at the user side (7),

$$P\left(\phi^{U}\right) = \frac{(2\pi)^{-2n}D^{-n}}{\Omega} \frac{\exp\left[\kappa\cos\left(\phi^{U}-\mu\right)\right]}{\pi I_0(\kappa)} \times \int\limits_{R_1}^{R_2} R^{-n}\left(1 - n\frac{R}{D}\cos\left(\phi^{U}\right)\right) f(R)dR, \quad \phi^{U} \in [-\pi,\pi). \tag{7}$$

The PAS seen by the BS can be derived similarly by setting $a = b_{lm} = z = 0$, $\Delta\delta = \delta_{pq}$ and $\tilde{\phi} = \alpha_{pq}$ in (5). The final result is given by (8).

C. PDF of Time of Arrival

From the trigonometric relations in [6, eq. (9)], Fig. 1 and under the assumption of $D \gg R$, $\forall R \in [R_1, R_2]$, the travel time of a wave originated from the BS, reflected from the scatterer with the position defined by R and ϕ^U, and received by the user, can be approximated by $\tau \approx \left(R + D + R\cos\left(\phi^{U}\right)\right)/c$. Upon modeling the user AOA with the von Mises PDF in (4), transformation of the random variable ϕ^U using previous relation can give us the conditional PDF of the relative TOA $f\left(\tau_r\,|\tau_R^{\max}\right)$ for a given radius R or, correspondingly, the maximum relative delay $\tau_R^{\max} = 2R/c$. The relative delay is defined as $\tau_r = \tau - \tau_{LOS}$ and $\tau_{LOS} = D/c$ is the LOS delay. Calculating the TOA PDF is straightforward (9), where $\tau_{R_1}^{\max} = 2R_1/c$ and $\tau_{R_2}^{\max} = 2R_2/c$. For a given $f\left(\tau_R^{\max}\right)$, this integral can be calculated numerically.

D. Power Delay Spectrum

The correlation function $R_T(\Delta f, \Delta t)$ is defined as

$$R_T(\Delta f, \Delta t) = E\left[T^*(f,t)T(f+\Delta f, t+\Delta t)\right] \tag{10}$$

and from (3) and (5) equals to $\Omega\rho(\Delta f, \Delta t)$ for $b_{lm} = c_{pq} = 0$.

The PDS $P(\tau)$ is the inverse FT of the frequency correlation $R_T(\Delta f, \Delta t = 0)$ [11], i.e., $P(\tau) = \mathcal{F}^{-1}_{\Delta f}\{R_T(\Delta f)\}$. Substitution of (10) and (5) into the definition of PDS gives (11) after the FT and extensive calculations.

$$f(\tau_r) \approx \begin{cases} \int_{\tau_{R_1}^{\max}}^{\tau_{R_2}^{\max}} \exp\left[\kappa(2\tau_r/\tau_R^{\max}-1)\cos(\mu)\right] \frac{\cosh\left[2\kappa\sqrt{(1-\tau_r/\tau_R^{\max})\tau_r/\tau_R^{\max}}\sin(\mu)\right]}{\pi\tau_R^{\max} I_0(\kappa)\sqrt{(1-\tau_r/\tau_R^{\max})\tau_r/\tau_R^{\max}}} f(\tau_R^{\max})d\tau_R^{\max}, 0 \le \tau_r \le \tau_{R_2}^{\max} \\ \int_{\tau_r}^{\tau_{R_2}^{\max}} \exp\left[\kappa(2\tau_r/\tau_R^{\max}-1)\cos(\mu)\right] \frac{\cosh\left(2\kappa\sqrt{(1-\tau_r/\tau_R^{\max})\tau_r/\tau_R^{\max}}\sin(\mu)\right)}{\pi\tau_R^{\max} I_0(\kappa)\sqrt{(1-\tau_r/\tau_R^{\max})\tau_r/\tau_R^{\max}}} f(\tau_R^{\max})d\tau_R^{\max}, \tau_{R_1}^{\max} < \tau_r \le \tau_{R_2}^{\max}, \end{cases} \tag{9}$$

$$P(\tau_r) \approx \begin{cases} \frac{(2\pi)^{-2n}(cD/2)^{-n}}{\pi I_0(\kappa)} \int_{\tau_{R_1}^{\max}}^{\tau_{R_2}^{\max}} \left(1 - n\frac{\tau_r - \tau_R^{\max}/2}{\tau_{LOS}}\right) \exp\left(\frac{\kappa}{\tau_R^{\max}}\cos(\mu)\left(2\tau_r - \tau_R^{\max}\right)\right) \\ \qquad \times \frac{\cosh\left(2\kappa\sin(\mu)\sqrt{\tau_r(\tau_R^{\max}-\tau_r)}/\tau_R^{\max}\right)}{\sqrt{\tau_r(\tau_R^{\max}-\tau_r)}} (\tau_R^{\max})^{-n} f(\tau_R^{\max})d\tau_R^{\max}, \qquad 0 \le \tau_r \le \tau_{R_1}^{\max} \\ \frac{(2\pi)^{-2n}(cD/2)^{-n}}{\pi I_0(\kappa)} \int_{\tau_r}^{\tau_{R_2}^{\max}} \left(1 - n\frac{\tau_r - \tau_R^{\max}/2}{\tau_{LOS}}\right) \exp\left(\frac{\kappa}{\tau_R^{\max}}\cos(\mu)\left(2\tau_r - \tau_R^{\max}\right)\right) \\ \qquad \times \frac{\cosh\left(2\kappa\sin(\mu)\sqrt{\tau_r(\tau_R^{\max}-\tau_r)}/\tau_R^{\max}\right)}{\sqrt{\tau_r(\tau_R^{\max}-\tau_r)}} (\tau_R^{\max})^{-n} f(\tau_R^{\max})d\tau_R^{\max}, \qquad \tau_{R_1}^{\max} < \tau_r \le \tau_{R_2}^{\max} \end{cases} \tag{11}$$

V. Comparison with Measured Data

In order to validate our model, we compare the properties of the circular ring structure derived in Section IV with the experimental data available in [13]. In this paper we use the data set collected at the location of Aarhus with the BS antenna mounted at 12 m above the average rooftop level (high antenna position), since only for that one all the measured data are presented in [13]. In most cases, there was no LOS between the MS and BS.

In the sequel, we have tried to find a single set of parameters $\{\kappa, \mu, D, R_2, R_1\}$ that gives a reasonably good fit for all the four measured channel functions. To calculate the AOA PDF, PAS, TOA PDF and PDS in (6), (8), (9) and (11), respectively, numerical integration should be carried out for any $f(R)$, or correspondingly, for any $f(\Delta)$ or $f(\tau_R^{\max})$. We assume throughout the paper that $f(R) = 2R/(R_2^2 - R_1^2)$, which together with the special case of $f(\phi^U) = 1/2\pi$, i.e., $\kappa = 0$ in (4), gives uniformly distributed scatterers within the circular ring area. The value of $\mu = 180^\circ$ was chosen based on the layout. The path-loss exponent was set to $n = 1$. The set of parameters that shows a reasonable fit is $\kappa = 2$, $D = 2300$, $R_2 = 549$ m and $R_1 = 54.9$ m, as depicted in Fig. 2 and 3. The numerical simulations are added to the plots in order to show the accuracy of derived theoretical expressions.

Azimuthal characteristics, the AOA PDF and PAS seen by the BS are given in Fig. 2. Fig. 2(a) shows the comparison of the PDF in AOA of the circular ring model given in (6) and the measured data given by [13, Fig. 10]. The PAS represents distribution of the received power at the BS in terms of the azimuth angle and it is shown in Fig. 2(b). The curve obtained from (8) is normalized such that the maximum value is set to the relative power of 0 dB. The measured data is reported in [13, Fig. 4].

Temporal (delay) characteristics are given by Fig. 3. Comparison between the PDF in TOA for the circular ring model given by (9) and the measured data is given in Fig. 3(a). The histogram of data collected from the measurement campagne [13, Fig. 11] is converted into the PDF. Finally, Fig. 3(b) shows the comparison of the PDS of the circular ring model in (11) with the empirical curve given in Fig. 6 of [13]. The theoretical and experimental PDS curves are normalized such that the area under both is unity. The measured RMS delay spread of 0.4 μs is reported [13]. The RMS delay spread is defined as $\tau_{RMS} = \sqrt{\bar{\tau}^2 - \bar{\tau}^2}$, and for the circular ring model is calculated to be 0.47 μs.

Note that the PDS of the circular ring model presented in Fig. 3(b) is quite linear in some regions, $\tau_N \approx 0.5$, for example. This linear region resembles the widely used exponential distribution for the PDS [13]. It is clear that by choosing the parameters properly, the circular ring model provides good match to several key channel functions of interest.

VI. Conclusion

In this paper we have proposed the circular ring model for outdoor wideband MIMO mobile fading channels. This model provides a generic space-time-frequency (STF) correlation structure, suitable for characterization and simulation of STF selective MIMO channels. Moreover, it provides a simple yet realistic environment for comparative performance analysis of coding/detection techniques. Relevant channel functions of the circular ring model are also derived and compared with the published data in the literature. The close fit between the empirical data and theoretical results demonstrates the utility of our model for wideband MIMO channels.

References

[1] J. H. Winters, "On the capacity of radio communications systems with diversity in rayleigh fading environments," *IEEE J. Select. Areas Commun.*, vol. 5, pp. 871–878, June 1987.

[2] I. E. Telatar, "Capacity of multi-antenna gaussian channels," *European Trans. Telecommun. Related Technol.*, vol. 10, pp. 585–595, 1999.

[3] G. J. Foschini and M. J. Gans, "On limits of wireless communications in fading environments when using multiple antennas," *Wireless Personal Commun.*, vol. 6, pp. 311–335, 1998.

[4] A. Naguib, N. Seshadri, and A. Calderbank, "Increasing data rate over wireless channels," *IEEE Signal Processing Mag.*, vol. 17, pp. 76–92, 2000.

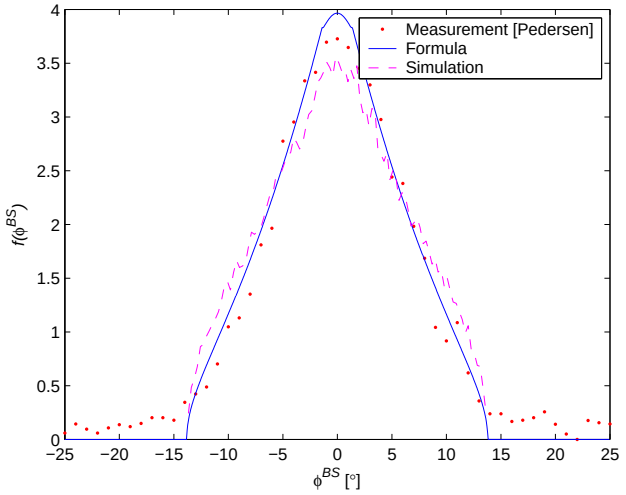

(a) Comparison of the AOA PDF seen by the BS for the circular ring model with measurements [13, Fig. 10].

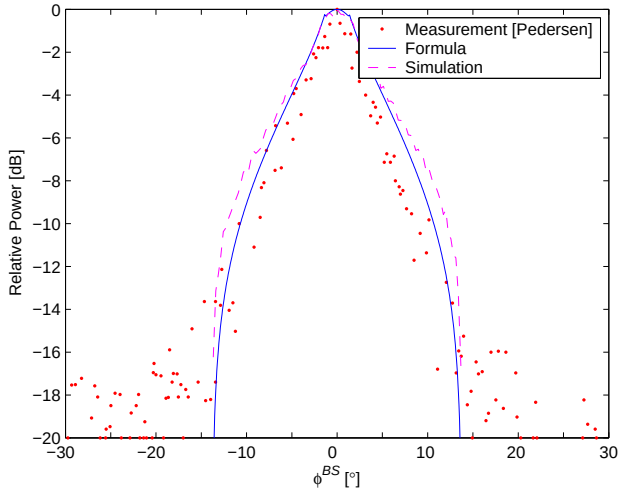

(b) Comparison of the PAS seen by the BS for the circular ring model with measurements [13, Fig. 4, Aarhus, high antenna position].

Fig. 2. Azimuthal characteristics seen by the BS.

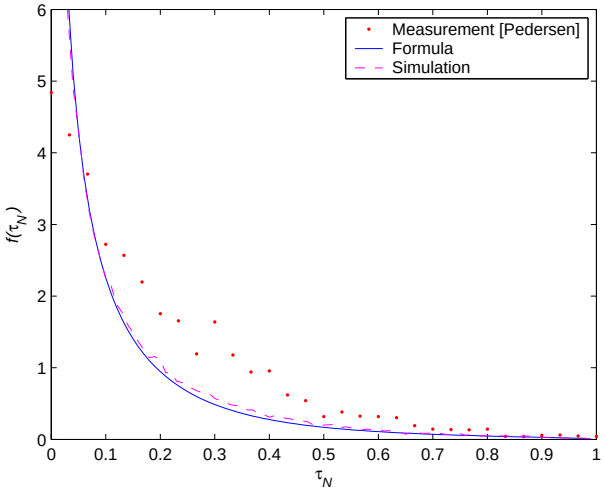

(a) Comparison of the TOA PDF for the circular ring model with measurements [13, Fig. 11].

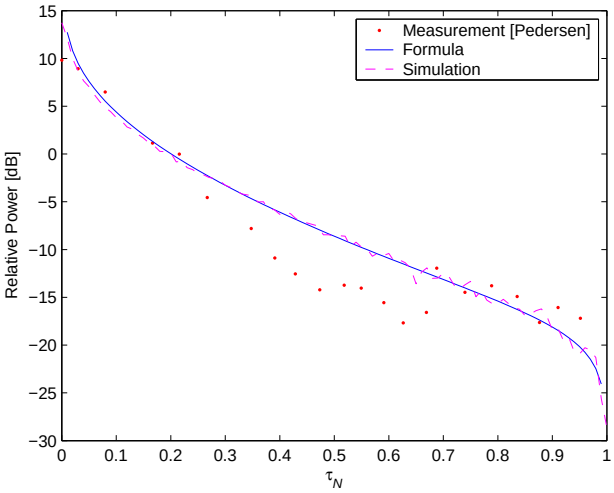

(b) Comparison of the PDS for the circular ring model with measurements [13, Fig. 6, Aarhus, high antenna position].

Fig. 3. Temporal (delay) characteristics.

[5] A. Paulraj, D. Gore, R. Nabar, and H. Bolcskei, "An overview of mimo communications-a key to gigabit wireless," *Proc. IEEE*, vol. 92, pp. 198–218, 2004.

[6] Z. Latinovic, A. Abdi, and Y. Bar-Ness, "A wideband space-time model for mimo mobile fading channels," in *Proc. IEEE Wireless Commun. Networking Conf.*, New Orleans, LA, 2003, pp. 338–342.

[7] W. C. Jakes Jr., *Microwave Mobile Communications*. Piscataway, NJ: IEEE Press, 1993.

[8] G. L. Stuber, *Principles of Mobile Communications*. Boston, MA: Kluwer, 2001.

[9] T. A. Chen, M. P. Fitz, W. Y. Kuo, M. D. Zoltowski, and J. H. Grimm, "A space-time model for frequency nonselective rayleigh fading channels with applications to space-time modems," *IEEE J. Select. Areas Commun.*, vol. 18, pp. 1175–1190, 2000.

[10] W. C. Y. Lee, "Effects on correlation between two mobile radio base station antennas," *IEEE Trans. Commun.*, vol. 21, pp. 1214–1224, 1973.

[11] P. A. Bello, "Characterization of randomly time-variant linear channels," *IEEE Trans. Commun. Sys.*, vol. 11, pp. 360–393, 1963.

[12] B. H. Fleury, "First- and second-order characterization of direction dispertion and space selectivity in the radio channel," *IEEE Trans. Inform. Theory*, vol. 46, pp. 2027–2044, 2000.

[13] K. I. Pedersen, P. E. Mogensen, and B. H. Fleury, "A stochastic model of the temporal and azimuthal dispersion seen at the base station in outdoor propagation environments," *IEEE Trans. Veh. Technol.*, vol. 49, pp. 437–447, 2000.

[14] A. Erdelyi, Ed., *Tables of integral transforms*. New York, NY: McGraw-Hill, 1954, vol. 1.